JACS
JOURNAL OF THE AMERICAN CHEMICAL SOCIETY

Article

pubs.acs.org/JACS

GFP-Like Phototransformation Mechanisms in the Cytotoxic Fluorescent Protein KillerRed Unraveled by Structural and Spectroscopic Investigations

Eve de Rosny[†] and Philippe Carpentier*[,‡]

[†]Institut de Biologie Structurale Jean-Pierre Ebel, Groupe Métalloprotéines, UMR 5075, Université Joseph Fourier Grenoble 1, CEA, CNRS, 41 rue Horowitz, 38027, Grenoble Cedex 1, France

[‡]Structural Biology Group, European Synchrotron Radiation Facility, 6 Rue Jules Horowitz, 38043, Grenoble Cedex 9, France

Supporting Information

ABSTRACT: KillerRed (KR) is a red fluorescent protein recognized as an efficient genetically encoded photosensitizer. KR generates reactive oxygen species *via* a complex process of photoreactions, ending up in photobleaching, the mechanism of which remains obscure. In order to clarify these mechanisms, we focus on a single mutant V44A (A44-KR) exhibiting the solely green component of KR. We report on the laser-induced structural transformations of A44-KR at cryogenic temperature, which we have investigated by combining UV−vis fluorescence/absorption spectroscopy with X-ray crystallography. Like the well-known GFP, A44-KR possesses a mixture of protonated (A) absorbing at 397 and deprotonated (B) absorbing at 515 nm chromophores, which are stressed by intense prolonged violet and blue laser sources. Both illuminations directly drive the B-chromophores toward a bleached *trans* isomerized form. A-type chromophores are sensitive only to violet illumination and are phototransformed either into a deprotonated green fluorescent form by decarboxylation of E218 or into a bleached form with a disordered *p*-hydroxybenzylidene. *In crystallo* spectroscopy at cryo-temperature allowed the identification and dissection of an exhaustive scheme of intermediates and end-products resulting from the phototransformation of A44-KR. This constitutes a framework for understanding the photochemistry of the photosensitizer KillerRed.

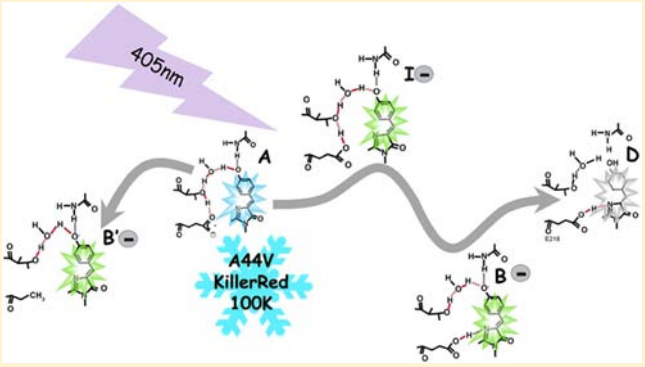

INTRODUCTION

The discovery of GFP (green fluorescent protein) has stimulated a vast development of the use of fluorescent proteins (FPs) for imaging techniques in molecular and cell biology. FPs undergo irreversible phototransformations upon intense illumination that modify their fluorescence properties. Such intense light inducing chemical reactions is defined as actinic light. These transformations include photoconversion from one fluorescence emission bandwidth to another, photoactivation from dark to fluorescent states, and photobleaching from fluorescent to dark states. As an example, GFP and its photoactivatable mutant (PA-GFP) undergo photoconversion and photoactivation processes, respectively. In both cases the chromophore is deprotonated upon intense prolonged UV/blue illumination *via* E222 decarboxylation.[1−4] Overilluminated FPs definitely succumb to photobleaching, a major inconvenience in imaging techniques that has, however, been turned into an advantage for some applications such as fluorescence recovery after photobleaching (FRAP).[5] Irreversible phototransformations originate from chemical and structural modifications internal to chromophores and/or of their local environments. Even though the molecular mechanisms for irreversible photoconversion and activation are well described for several FPs,[3,6−9] the structural basis of the photobleaching process remains poorly characterized. FPs are subject to a wide range of photosensitivities, and it is essential to understand the principle of photobleaching mechanisms to rationally design photoresistant or highly sensitive mutants, depending on the imaging application. KillerRed (KR) is a powerful photosensitizer used in the chromophore-assisted light inactivation (CALI) technique and for light-induced cell-killing experiments.[10] The cytotoxic mechanism has been fairly well studied[11−14] and involves an electron transfer mediated photosensitizing mechanism[15] that is associated with the bleaching of the red chromophores into a green protonated form.[11,16,17] The coexistence of green and red species in KR indicates that the maturation of the red chromophore, essential for cytotoxicity, is systematically incomplete or unstable.[16,18] Such incomplete maturation was already noticed for the red

Received: July 26, 2012
Published: October 1, 2012

   dx.doi.org/10.1021/ja3073337 | *J. Am. Chem. Soc.* 2012, 134, 18015−18021

fluorescent protein DsRed.[19] Recently we and others[16,17] showed that a single mutation in the vicinity of the chromophore (A44V or E68Q) completely destabilizes or inhibits the red maturation of KR, resulting in a solely GFP-like emitting protein that has lost its cytotoxicity.[16] In KR, ROS are generated upon actinic green/yellow illumination[10] of the red chromophores, which are converted in prebleached green forms.[11] In this work, we investigate the subsequent stages of photobleaching by combining single crystal fluorescence/absorption spectroscopy at cryo-temperature with structural data on the spectrally simplified A44V green mutant (A44-KR). This allowed the elucidation of the complete molecular mechanisms of laser-induced photoconversion and photobleaching of the green species of KR. The characterization of the green-range phototransformation scheme together with the analysis of the structural differences between the cytotoxic KR and its bleached-like form A44-KR bring forth new elements on the ROS release process, which is essential to the cytotoxicity.

EXPERIMENTAL SECTION

Cloning, Expression, and Purification. The V44A KillerRed mutant, cloned into the pet15-b vector (Novagen), was obtained as previously described.[17] It was expressed in *Escherichia coli* BL21-(DE3)pLysS and purified on a cobalt affinity column chromatography (Talon, Clontech) using a 15 to 300 mM imidazole gradient, followed by a gel filtration on a High Load 16/60 Superdex 75 prep grade column (Amersham Biosciences) equilibrated with 50 mM Hepes pH7.5.

Crystallization. Crystals of A44-KR were obtained using the hanging drop vapor diffusion method with the conditions described in the Supporting Information (Figure S8).

***In Crystallo* Spectroscopy.** Absorption/fluorescence spectra of the A44-KR crystals were collected at 100 K. Crystals (100 × 100 × 400 μm^3) were mounted in standard spine supports using the "off-line" microspectrophotometer at the laboratory Cryobench (ESRF) for all phototransformation kinetic studies[20] and using the "on-line" microspectrophotometer installed on the beamline ID14-eh1 (ESRF) to produce and monitor *in situ* the phototransformation of crystals for X-ray studies.[21] The spectra were recorded with a compact fiber optic CCD spectrometer (HR2000+, Ocean Optics, Dunedin, FL, USA). Fluorescence excitation and actinic illumination were carried out using either a 405 nm CW laser (OZ-Optics, Ottwa, Ontario Canada) or a 473 nm CW laser (MBL-III-473, CNI, Changchun China). The focal spot diameter was set to 50 μm for the "off-line" experiments (405 nm/1.2 kW cm^{-2} and 473 nm/2.0 kW cm^{-2}) and to 125 μm for the "on-line" experiments (405 nm/0.2 kW cm^{-2} and 473 nm/0.3 kW cm^{-2}). The absorption spectra were measured using a balanced broad UV–vis source (DH2000-BAL, Ocean Optics, Dunedin, FL, USA) with an acquisition time of 50 ms. The fluorescence was excited by short laser pulses (405 nm or 473 nm) of 5 ms, and the spectra were collected at 90° from the axis of excitation.[20] The different phototransformation processes were monitored by a series of long actinic illumination (405 or 473 nm) periods of 10 s, interleaved with short spectra acquisitions time (absorption or fluorescence). The series of spectroscopic data were computed by our own software tools (in Fortran language), applying a linear correction to the background. The kinetics consists of following the mean value of absorption or fluorescence integrated in a specific band, with a further correction from a collective background contribution for the absorption. The absorption B-bands were deconvolutued, using the commercial software PeakFit (SeaSolve Software Inc., San Jose, CA), by fitting 3 normal-log functions centered at 509, 511, and 515 nm, to resolve the contribution of each individual band to the overall peak. The details of the deconvolution are illustrated in Supplementary Figure S9, and results and statistics are compiled in Supplementary Table S1. The time evolutions of fluorescence upon actinic illuminations are presented in Supplementary Figures S10 and S11.

X-ray Data Collection. All Data sets were collected at the European Synchrotron Radiation Facility (ESRF) on beamline ID14-eh1 (Energy 13.27 keV) using an ADSC Q210 CCD detector (ADSC, California, USA). The X-ray beam size was adjusted so that it was smaller than the laser spot size to ensure probing exclusively phototransformed matter for the "on-line" experiments. Diffraction images were integrated and scaled with the XDS program package.[22] The native structure of A44-KR (PDB deposition 4b30) was solved by molecular replacement using PHASER[23] with KillerRed (PDB 2WIQ) as a starting model; the model has been built using coot[24] and refined using REFMAC5[23] against a reference data set collected to 2.1 Å. The difference electron density maps ($F^i_{obs} - F^j_{obs}$) between the different phototransfomation states of A44-KR were calculated with CNS[25,26] using the phase of the native structure and the Bayesian q-weighting of the difference structure factor amplitudes.[27] The chromophore geometry of A44-KR was observed to undergo a marked distortion upon X-ray absorption as previously described for IrisFP.[28] Therefore, each difference density map was calculated from 2 data sets recorded on the same crystal to minimize the defects of isomorphism, but at 2 different locations with strictly the same absorbed doses[29] so as to exactly compensate the contribution of the X-ray induced structural modifications (see Supplementary Table S2 for data collection strategies). All data collection and refinement statistics are summarized in Supplementary Table S3.

RESULTS AND DISCUSSION

Native A44-KR Single Crystal Structure and Spectroscopy. A44-KR crystallizes in the space group $P6_2$, with a dimer in the crystallographic asymmetric unit. The arrangement between the two monomers (namely I and II, Supplementary Figure S1) is isomorphous to that of KR and probably very similar to that in solution, since it is stabilized by strong contacts described in a former structural study.[16] Interestingly, the head-to-tail (−180°) orientation of the 2 chromophores, separated by 26 Å in the dimer, favors an internal FRET effect (Förster resonance energy transfer), providing that those fluorophores have the complementary spectral properties to constitute a donor–acceptor pair. The overall monomer structure of A44-KR is an 11-stranded β-barrel typical of the GFP family housing a chromophore maturated from the N-Y-G sequence at the middle of an internal α-helix standing along the barrel axis. It differs from the original KR by subtle but significant details in the chromophore environment. Like its precursor, A44-KR displays the remarkable long internal channel containing a continuous chain of hydrogen-bonded water molecules that connects the chromophore with the bulk solvent at the "bottom-cap" of the protein (Supplementary Figure S2). This channel, a feature unique among FP structures, is proposed to play an essential role in the cytotoxity of KR by mediating the traffic of oxygen species in and out of the protein or by acting as a proton wire.[13,16,17] The superimposition of the different monomers of KR structures (PDB 2WIQ, 3GB3) with those of A44-KR (Supplementary Figure S2) reveals that the water molecule Sol3 is only present in the structure of the red-maturated KR where it has a noticeably scattered location, indicating that this molecule is not strongly stabilized. Sol3 sits beneath the chromophore methylene bond and bridges the long chain of water molecules to E218. Its absence in A44-KR avails free space beneath the chromophore. The moderate 2.1 Å resolution of our structure does not allow discrimination between the expected single bond Cα-N65 of the green A44-KR and the fully red-maturated acylimine double bond. However, the non-maturation of A44-KR is unambiguously

established by spectroscopy (see below). Interestingly, E68, which corresponds to the catalytic residue S69 in DsRed,[30,31] exhibits different conformations in KR when compared to A44-KR. In KR, the E68 carbonyl is turned away from the matured acylimine group. Pletnev et al.[16] pointed out the probable high reactivity of this negatively charged residue placed in a mainly hydrophobic environment. The E68 side chain in the A44-KR structure reveals two alternate conformations (Supplementary Figure S3). One is in an inactive position, while the other is in a suitable catalytic position (toward N65) to facilitate the deprotonated Cα intermediate formation on the route from green to red maturation, similar to S69 in DsRed.[30] The water molecule Sol2 observed "below" the five-membered ring of the chromophore in the structure of A44-KR (Supplementary Figure S2) is proposed to be the product of the red maturation process. This situation, which strongly resembles that of DsRed,[30] suggests that the red maturation process also occurs in A44-KR, but with a much lower yield and stability than for KR, as attested by the quasi-total suppression of the 580 nm "red" absorption band (see below). Clearly, the steric space released by the mutation V44A relaxes the van der Waals contacts and generate a dynamical instability with two predominant conformations for I64, which consequently affects the stability of the adjacent acylimine bond (Supplementary Figure S4). Importantly, T201 exhibits two alternate conformations in monomer II. In one position, the hydroxyl group forms the typical proton wire linking Y66 with E218 *via* the water molecule Sol1, as in the neutral A-form of GFP[32] (Figure 1). The other position corresponds to a deprotonated B-form

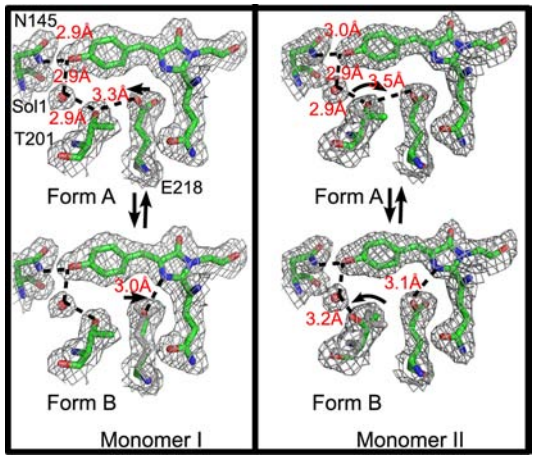

Figure 1. Environment of the 2 chromophores (monomers I and II) in the crystal structure of A44-KR. $2F_o - F_c$ electron density map is shown contoured at the 1σ level. Dashed lines represent possible hydrogen bonds. Alternate conformations of T201 observed in monomer II are represented in color and in gray.

since the H-bond network is clearly disrupted. Therefore, rotation of the T201 side chain appears as a structural mechanism that determines the chromophore protonation state. Even though a single conformation of T201 prevails in monomer I with an apparent typical GFP pattern, the bond lengths and the geometries suggest that E218 could be H-bonded, either to T201, corresponding to the neutral A-form, or to the nitrogen of the imidazolinone ring of the chromophore, which then corresponds to another deprotonated B-form (Figure 1). This suggests that a slight movement of the E218 side chain, not obviously resolvable in the 2.1 Å resolution structure, also constitutes a structural mechanism that discriminates the neutral from the anionic form.

The absorption spectrum of A44-KR in single a crystal at cryo-temperature is similar to that previously reported in solution.[16,17] It exhibits two major peaks at 397 and 515 nm (Figure 2A) corresponding to the protonated A- and deprotonated B-forms, respectively, as described for GFP.[32] This observation is consistent with our structural data revealing the two forms of the chromophore.

The quasi-absence of red maturated chromophores in the crystal is evidenced by a very weak absorption at 584 nm. Excitation of the B-form chromophore at 473 nm results in a single fluorescence emission with a maximum at 525 nm (Figure 3A), whereas excitation of the A-form with a 405 nm source gives rise to two emission peaks at 490 and 520 nm (Figure 3B, in dark blue).

This green emission peak (520 nm) can originate either from an excited state proton transfer (ESPT) process as in GFPs or from FRET between the neutral and the deprotonated forms in dimers owing to the distance and the relative orientation of the two chromophores (Supplementary Figure S1).

Phototransformation of the Deprotonated B-form. A prolonged intense illumination of a cryo-cooled native A44-KR crystal using a 473 nm laser produces a drastic reduction of the absorption of the B-form (515 nm), while the absorbance of the A-form (397 nm) remains unchanged (Figure 2B). This actinic light also reduces the green fluorescence (excitation 473 nm, Figure 3A). Both declines follow similar two-rate kinetics, with a fast phase lasting 5 min followed by slow process on the hour time scale (inset Figures 2B and 3A), revealing the bleaching of the B-form. The invariance of the 397 nm absorption band indicates not only that the A-form population is unaffected but also that there is no phototransformation of B into A. Counterintuitively, the blue fluorescence arising from A (excitation 405 nm) undergoes a significant increase (Figure 3B), rising from ~25% to ~60% of the total fluorescence (inset Figure 3B); this obviously depends only on the disappearance of B. This phenomenon is actually the consequence of the loss of the intradimeric energy transfer from A to B, which releases the blue fluorescence of A. It demonstrates that the A44-KR green fluorescence emitted upon excitation of A originates partly from the emission of B induced by FRET. Indeed, remaining green fluorescence (~30% of the total fluorescence) is still observed in the absence of FRET, when B is completely bleached (Figure 3B), confirming that the A emits green light by low rate ESPT.

The molecular modifications resulting from the phototransformation of the deprotonated B-form using a 473 nm actinic illumination were assessed by examining the difference Fourier electron density map. Figure 4A and B shows essentially that the *cis* chromophores isomerize at cryo-temperature. Such isomerization at cryo-temperature was recently denoted for the photoactivatable fluorescent protein Padron.[33] In A44-KR, the isomerization results in a strongly distorted *trans* conformation, obviously nonabsorbent. The lack of absorption suggests a disruption of the chromophore π-electron system that reduces its aromaticity, possibly subsequently to a photoinduced protonation of methylene groups, as evidenced for IrisFP.[28,34] During the photoisomerization movement, the chromophore pushes away the lateral chains of I163 and F177 by steric interactions. This overillumination appears to destabilize the H-bonding network that maintains the chromophore in its *cis* fluorescent state in

dx.doi.org/10.1021/ja3073337 | J. Am. Chem. Soc. 2012, 134, 18015−18021

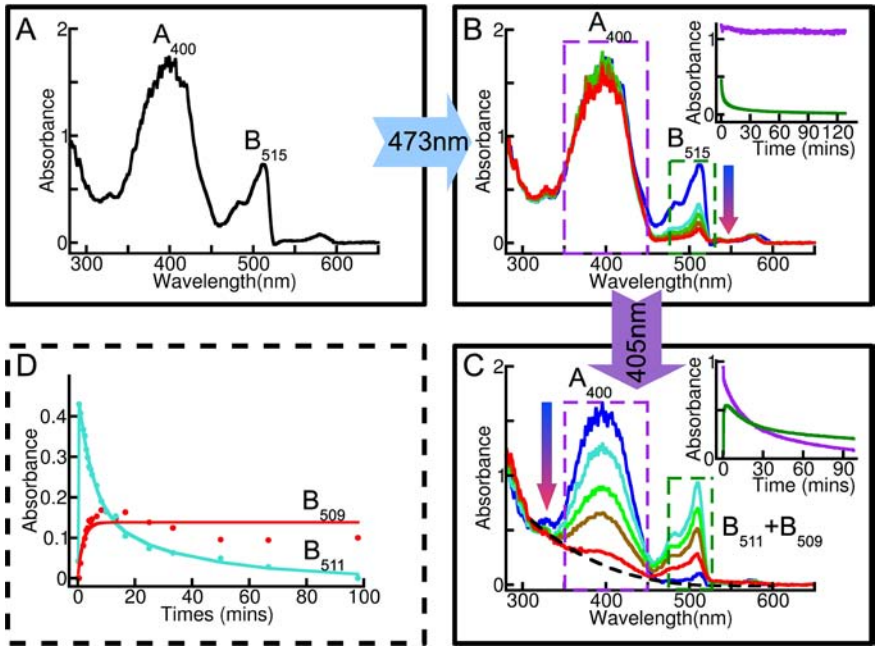

Figure 2. Phototransformations of A44-KR characterized by *in crystallo* absorption-spectroscopy. (A) Initial absorption spectrum from a single crystal of native A44-KR prior to illumination. (B) Time series (0, 200, 400, 800, 1600 s) of absorption spectra during 473 nm laser actinic illumination (power density 2.0 kW cm^{-2}). (C) Time series (0, 200, 800, 1600, 5900 s) of absorption spectra during subsequent 405 nm laser actinic illumination (power density 1.2 kW cm^{-2}). Black dashed line: polynomial fit of the baseline deviation. The insets in panels B and C represent the kinetics of the mean values of the absorption integrated in the 350−450 nm (purple) and 475−525 nm (green) bands. (D) Kinetics of the B-band deconvoluted in two components (B_{509} and B_{511}) during violet light overexposition.

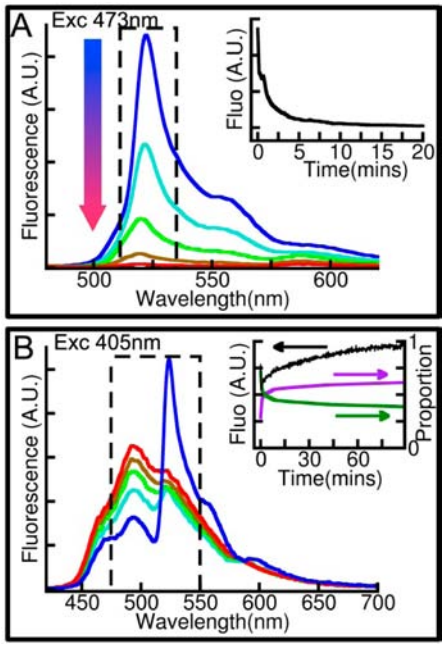

Figure 3. Kinetics of phototransformations of A44-KR characterized by *in crystallo* fluorescence spectroscopy during 473 nm laser actinic illumination (power density 2.0 kWcm^{-2}). (A) Excitation at 473 nm. Inset: kinetics of the mean intensity of the green fluorescence integrated in the 510−535 nm band. (B) Excitation at 405 nm. Inset: kinetic of the mean intensity integrated in the 475−550 nm band (black) with proportion of blue and green fluorescence (purple and green, respectively).

benefit of the *trans* side. Indeed, the N145T and T201I mutations have been reported to be indispensable for the evolution of the parental chomoprotein anm2CP into the cytotoxic KR.[11] The chromophore *cis*-isomer is stabilized by H-bonds with N145 and T201 *via* Sol1, while in the non-fluorescent amn2CP the chromophore was suggested to be in a *trans* form.[11,16,17] Strikingly, the actinic 473 nm illumination did not provoke the strong decarboxylation generally observed upon X-rays or UV−violet light overexposition,[2,3,6,7,28] but rather produced a displacement of E218 (Figure 4B).

Phototransformation of the Protonated A-form. The completely B-bleached crystal, arising from the above operation, was used to unambiguously follow the photo-transformation of the A-form. Subsequent 405 nm actinic illumination of the crystal provokes a reduction of the A absorption band with a biexponential kinetic (Figure 2C). A significant amount of green fluorescence upon 405 nm excitation remains when A is almost completely bleached (Supplementary Figure S10C), showing that the B-form is excitable by violet light, and therefore phototransformable, in its blue side absorption tail. The A-form decline is counter-balanced by a rapid appearance of a green absorption (within 1 min) that displays a maximum at 511 nm, indicating that A is phototransformed into a deprotonated species clearly different from the native B_{515}. This newly generated peak slowly disappears (hour time scale) with a progressive blue shift to 509 nm (Figure 2C). The deconvolution of the green absorption peak during the kinetic allows following the individual kinetic of two photogenerated species B_{511} and B_{509} that are spectroscopically different from the native B_{515}. B_{511} corresponds to the first abruptly generated species, which decreases until complete disappearance, whereas B_{509} increases slowly to reach saturation (Figure 2D). These kinetic profiles suggest that both species are different from the native B_{515} and arise from the A-form, B_{511} being an intermediate, as evidenced by its formation and consumption kinetic, on the way to bleaching and B_{509} an end

dx.doi.org/10.1021/ja3073337 | J. Am. Chem. Soc. 2012, 134, 18015−18021

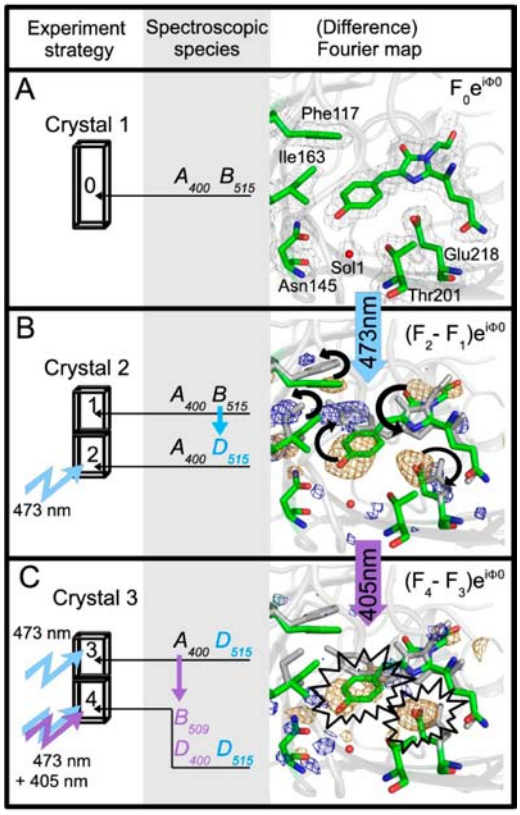

Figure 4. Structural characterization of the phototransformations of A44-KR. (Left column) Simplified experimental strategy (detailed in Supplementary Table S2). Two locations selected on each crystal are exposed or not to laser beams prior to X-ray datacollection and used for difference Fourier map calculations (ΔF_{obs} $e^{i\Phi}$). (Central column) Species identified by spectroscopy in each location. Colored arrows connect the species undergoing a phototransformation to their products (in blue, induced by a 473 nm laser and in violet by a 405 nm). (Right column) Difference maps between the two locations, revealing structural changes associated to phototransformations. (Row A) Native chromophore and its local environment in the $2F_o - F_c$ map contoured at 1σ (in gray) prior to actinic illumination. (Row B) Difference map (gold $-5.3\sigma/-3.3$ e Å^{-3}; blue $5.3\sigma/3.3$ e Å^{-3}) showing the molecular movements upon 473 nm overillumination. Black arrows indicate the movements from the native model (colored) to the bleached one (in gray). (Row C) Difference map (contoured at $\pm 6\sigma$/3.7 e Å^{-3}) highlighting molecular transformations upon 405 nm overillumination of an already 473 nm phototransformed crystal. Spark shapes emphasize the strongest disappearance of electron density.

product. The occurrence of an ESPT process, upon excitation at 405 nm, implies the formation of a transient deprotonated I intermediate.[35] It suggests that B_{511} arises from this intermediate by disruption of the proton wire between E218 and Y66.

The difference Fourier electron density map (Figure 4C) does not reveal any further isomerization of the A-form chromophore, as shown by the absence of negative density on the *trans*-conformer (previously generated by the photo-tranformation of B). The reduction of electronic density on the *p*-hydroxybenzylidene group of the *cis*-isomer suggests a structural destabilization probably due to photohydrogenation of the methylene bridge as observed for IrisFP.[28] In addition, E218 is strongly decarboxylated by the higher energy violet photons as compared to the 473 nm actinic light. This structural feature is consistent with our spectroscopic data revealing the photoconvertion of A into the final B_{509} form, as found for GFP in which E222 decarboxylation provokes the chomophore deprotonation.[3]

Concerted Phototransformation of A- and B-forms. The direct 405 nm actinic illumination of a native (untransformed) A44-KR crystal leads to the concerted transformation of the A- and B-forms. The resulting transformation is identical to that previously observed after the sequence of actinic illumination 473→405 nm. This combined transformation is highlighted in both spectroscopic and structural data (Supplementary Figures S5). The deconvolution of the green absorption peaks during the kinetic confirms the bleaching of native B_{515} concomitantly with the formation of B_{509} and transiently B_{511} species arising from the A-protonated chromophores of A44-KR. The Fourier difference map of the phototransformed protein reveals a *trans* isomerization of the chromophore as found after actinic illumination at 473 nm on the native crystal, which is in addition associated with the decarboxylation of E218 as found after actinic illumination at 405 nm. The absence of E218 detectable movement indicates that the decarboxylation yield provoked by the 405 nm source is very efficient.

CONCLUSIONS

In this study we have combined X-ray crystallography with *in crystallo* spectroscopy at cryogenic temperature on the A44V-KR mutant, in an attempt to investigate the laser-induced photoconversion and photobleaching of the green component of KillerRed. Structural information and absorption spectroscopy reveal that the coexistence of protonated and deprotonated chromophores in the native A44-KR depends on the rotamer state of T201 and possibly on the *anti*/*syn* conformation of the E218 side chain. The presence of a proton wire pattern (Y66−E218) is consistent with the emission of green fluorescence by the protonated A-form *via* an ESPT process. Altogether, these observations show that the green species of KillerRed resembles that of wt-GFP with T201 and E218 roles being equivalent to S205 and E222 in GFP.[32] We demonstrate that A44-KR is a highly photosensitive FP, which advantageously undergoes *in crystallo* multiple light-induced transformations. The intermediates and products of the reaction are stabilized at cryogenic temperature. We conclude with a complete mechanism of phototransformation provoked by actinic illuminations (Scheme 1 and Supplementary Figure S6).

Actinic lights, in the violet to cyan range, bleach the B_{515} chromophore to a unique *trans* isomerized D_{515} form, while A_{400} is only sensitive to the violet light. A_{400} is phototransformed either into a deprotonated B_{509} form *via* a E218-decarboxylation event or into the bleached D_{400} form with a disordered *p*-hydroxybenzylidene group. The spectroscopy results show that D_{400} is generated *via* 2 green intermediates: I (the GFP-like intermediate) and B_{511}. The latter species is generated by disruption of the H-bond between T201 and E218, which side chain switches from an *anti*- to *syn*-conformation and binds to the imidazolinone group. This low energy-barrier process can be trapped thanks to the cryogenic conditions. In previous experiments in which KR was bleached at room temperature prior to the X-ray experiments, the chromophore displayed the structural features of D_{400} with a disordered benzyliden group.[16,17] B_{509} appears to be photoresistant *in crystallo* at cryogenic temperature; however, it would probably be bleached at room temperature into a dark

dx.doi.org/10.1021/ja3073337 | J. Am. Chem. Soc. 2012, 134, 18015−18021

Scheme 1. Proposed Mechanism for the Phototransformation at 100 K of A44-KR Chromophores upon Actinic Illuminations (405, 473 nm)[a]

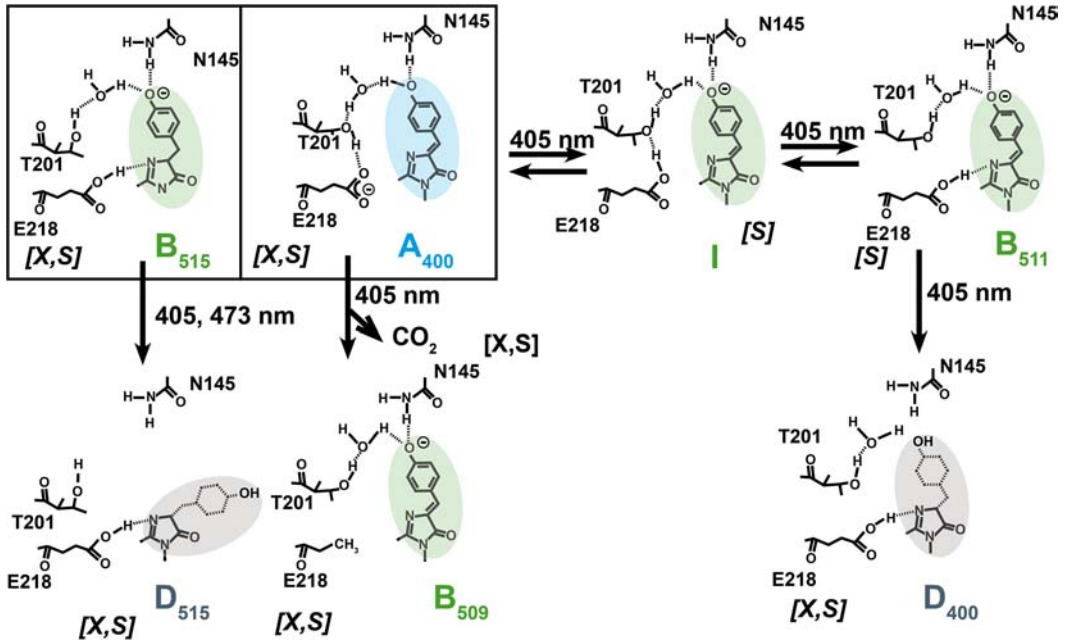

[a]The fluorescence emission of the different states is highlighted by colored halos (blue, green, or dark). Dotted benzyliden groups are nonconjugated. The initial native chromophores (green B_{515} and blue A_{400}) are marked out by a frame contour. *[X]*: characterized by crystallography, *[S]*: characterized by spectroscopy.

D_{509} species. The photobleaching sensitivity of A44-KR was shown to be related to the softness of the chromophore pockets, as evidenced by the photoinduced movements of the side chain residues involved in maintenance of the pseudorigidity of the chromophore in its *cis* fluorescence state.[11] These movements are irreversible and likely result in a stable nonfluorescent *trans* conformation. The softness of the chromophore pocket probably also contributes to the low fluorescence quantum yield of KillerRed (0.25),[11] consistent with the relatively distorted geometry of the chromophore.[16,19] We see clear evidence that actinic illumination at low energy (473 nm) results in molecular displacements, whereas deeper photochemical transformations are observed at higher energy (405 nm). Our data suggest that the photosensitivity of fluorescent proteins is in part related to the softness of the chromophore pocket and of the susceptibility of the methylene group to photochemical transformations. The GFP, which chromophore pocket is more rigid and exiguous than that of A44-KR, also undergoes a light-induced decarboxylation that is photon energy dependent;[2] however, it does not isomerize. As a matter of example a single mutation in the chromophore environment of EosFP (IrisFP) results in a wider pocket and allows isomerizations.[36]

In addition, our data reveal new insights into the mechanism of photobleaching that is responsible for the phototoxicity of KillerRed. It has been shown that ROS are generated upon bleaching of the red form using a green/yellow light.[10] These bleaching results in a protonated green chromophore[11] that likely corresponds to the A_{400} species described here. The comparison between KR and A44-KR allows us to propose that the water molecule Sol3 (Supplementary Figure S2), strategically situated close to the methylene bridge and belonging to the long chain of water molecules, can be involved in the protonation of the Cα atom. Indeed, as proposed for the dark state of IrisFP,[28,34] the loss of the double bond probably assists the isomerization and the bleaching of the chromophore. We also show that the photoinduced isomerization of the chromophore and disordering of the *p*-hydroxybenzylidene goup enhance the access of the chromophore pocket to the bulk solvent through the pore between the seventh and 10th β-strand of the barrel and probably improve the diffusion of the ROS generated during a prebleach operation.[11]

The non-cytotoxic mutant V44A of KillerRed could be a promising tool for imaging techniques and could serves as a basis upon which to engineer new fluorescent molecules with improved properties. This fluorescent protein, which is easily bleachable with blue/green laser sources, is a good candidate for FRAP experiments. In addition, at cryogenic temperatures, the green fluorescence can be switched off (bleaching of B chromophores) and recovered (phototransfomation of A chromophores into B_{509}). Such properties can be valuable in high-resolution fluorescence microscopy techniques and for further developments of low temperature techniques.[33] Finally, the dimeric FRET-pair allows the possibility of photoconversion from a green to a dual blue/green color-emitting protein (Supplementary Figure S7).

■ ASSOCIATED CONTENT

Supporting Information

This material is available free of charge via the Internet at http://pubs.acs.org.

■ AUTHOR INFORMATION

Corresponding Author

philippe.carpentier@esrf.fr

Notes

The authors declare no competing financial interest.

■ ACKNOWLEDGMENTS

We thank Dominique Bourgeois for insightful discussions concerning the precursor protein KillerRed, and we are grateful to Sébastien Violot who generated the A44V mutant protein. This work benefits from in-house research access to the beamline ID14-eh1 and to the "on-line" microspectrophotometer at the ESRF Grenoble. We thank Antoine Royant for helpful discussions and for user support at the laboratory Cryobench (ESRF) and Elspeth Gordon, Gordon Leonard, and Max Nanao for their contribution to the improvement of the quality of our manuscript.

■ REFERENCES

(1) Patterson, G. H.; Lippincott-Schwartz, J. *Science* **2002**, *297*, 1873.
(2) Bell, A. F.; Stoner-Ma, D.; Wachter, R. M.; Tonge, P. J. *J. Am. Chem. Soc.* **2003**, *125*, 6919.
(3) van Thor, J. J.; Gensch, T.; Hellingwerf, K. J.; Johnson, L. N. *Nature Struct. Biol.* **2002**, *9*, 37.
(4) Henderson, J. N.; Gepshtein, R.; Heenan, J. R.; Kallio, K.; Huppert, D.; Remington, S. J. *J. Am. Chem. Soc.* **2009**, *131*, 4176.
(5) Day, R. N.; Davidson, M. W. *Chem. Soc. Rev.* **2009**, *38*, 2887.
(6) Habuchi, S.; Cotlet, M.; Gensch, T.; Bednarz, T.; Haber-Pohlmeier, S.; Rozenski, J.; Dirix, G.; Michiels, J.; Vanderleyden, J.; Heberle, J.; De Schryver, F. C.; Hofkens, J. *J. Am. Chem. Soc.* **2005**, *127*, 8977.
(7) Subach, F. V.; Malashkevich, V. N.; Zencheck, W. D.; Xiao, H.; Filonov, G. S.; Almo, S. C.; Verkhusha, V. V. *Proc. Natl. Acad. Sci. U.S.A.* **2009**, *106*, 21097.
(8) Hayashi, I.; Mizuno, H.; Tong, K. I.; Furuta, T.; Tanaka, F.; Yoshimura, M.; Miyawaki, A.; Ikura, M. *J. Mol. Biol.* **2007**, *372*, 918.
(9) Nienhaus, K.; Nienhaus, G. U.; Wiedenmann, J.; Nar, H. *Proc. Natl. Acad. Sci. U.S.A.* **2005**, *102*, 9156.
(10) Bulina, M. E.; Lukyanov, K. A.; Britanova, O. V.; Onichtchouk, D.; Lukyanov, S.; Chudakov, D. M. *Nat. Protoc.* **2006**, *1*, 947.
(11) Bulina, M. E.; Chudakov, D. M.; Britanova, O. V.; Yanushevich, Y. G.; Staroverov, D. B.; Chepurnykh, T. V.; Merzlyak, E. M.; Shkrob, M. A.; Lukyanov, S.; Lukyanov, K. A. *Nat. Biotechnol.* **2006**, *24*, 95.
(12) Mueller, G.; Waldeck, W.; Braun, K. *J. Photochem. Photobiol., B* **2010**, *98*, 95.
(13) Roy, A.; Carpentier, P.; Bourgeois, D.; Field, M. *Photochem. Photobiol. Sci.* **2010**, *9*, 1342.
(14) Jacobson, K.; Rajfur, Z.; Vitriol, E.; Hahn, K. *Trends Cell Biol.* **2008**, *18*, 443.
(15) Vegh, R. B.; Solntsev, K. M.; Kuimova, M. K.; Cho, S.; Liang, Y.; Loo, B. L.; Tolbert, L. M.; Bommarius, A. S. *Chem. Commun. (Cambridge, U. K.)* **2011**, *47*, 4887.
(16) Pletnev, S.; Gurskaya, N. G.; Pletneva, N. V.; Lukyanov, K. A.; Chudakov, D. M.; Martynov, V. I.; Popov, V. O.; Kovalchuk, M. V.; Wlodawer, A.; Dauter, Z.; Pletnev, V. *J. Biol.l Chem.* **2009**, *284*, 32028.
(17) Carpentier, P.; Violot, S.; Blanchoin, L.; Bourgeois, D. *FEBS Lett.* **2009**, *583*, 2839.
(18) Nordgren, M.; Wang, B.; Apanasets, O.; Brees, C.; Veldhoven, P. P.; Fransen, M. *J. Microsc.* **2012**, *245*, 229.
(19) Gross, L. A.; Baird, G. S.; Hoffman, R. C.; Baldridge, K. K.; Tsien, R. Y. *Proc. Natl. Acad. Sci. U.S.A.* **2000**, *97*, 11990.
(20) Royant, A.; Carpentier, P.; Ohana, J.; McGeehan, J.; Paetzold, B.; Noirclerc-Savoye, M.; Vernede, X.; Adam, V.; Bourgeois, D. *J. Appl. Crystallogr.* **2007**, *40*, 1105.
(21) McGeehan, J.; Ravelli, R. B.; Murray, J. W.; Owen, R. L.; Cipriani, F.; McSweeney, S.; Weik, M.; Garman, E. F. *J. Synchrotron Radiat.* **2009**, *16*, 163.
(22) Kabsch, W. *Acta Crystallogr., Sect. D: Biol. Crystallogr.* **2010**, *66*, 125.
(23) Winn, M. D.; Ballard, C. C.; Cowtan, K. D.; Dodson, E. J.; Emsley, P.; Evans, P. R.; Keegan, R. M.; Krissinel, E. B.; Leslie, A. G.; McCoy, A.; McNicholas, S. J.; Murshudov, G. N.; Pannu, N. S.; Potterton, E. A.; Powell, H. R.; Read, R. J.; Vagin, A.; Wilson, K. S. *Acta Crystallogr., Sect. D: Biol. Crystallogr.* **2011**, *67*, 235.
(24) Emsley, P.; Cowtan, K. *Acta Crystallogr., Sect. D: Biol. Crystallogr.* **2004**, *60*, 2126.
(25) Brunger, A. T.; Adams, P. D.; Clore, G. M.; DeLano, W. L.; Gros, P.; Grosse-Kunstleve, R. W.; Jiang, J. S.; Kuszewski, J.; Nilges, M.; Pannu, N. S.; Read, R. J.; Rice, L. M.; Simonson, T.; Warren, G. L. *Acta Crystallogr., Sect. D: Biol. Crystallogr.* **1998**, *54*, 905.
(26) Brunger, A. T. *Nat. Protoc.* **2007**, *2*, 2728.
(27) Ursby, T.; Bourgeois, D. *Acta Crystallogr., Sect. A* **1997**, *53*, 564.
(28) Adam, V.; Carpentier, P.; Violot, S.; Lelimousin, M.; Darnault, C.; Nienhaus, G. U.; Bourgeois, D. *J. Am. Chem. Soc.* **2009**, *131*, 18063.
(29) Paithankar, K. S.; Owen, R. L.; Garman, E. F. *J. Synchrotron Radiat.* **2009**, *16*, 152.
(30) Yarbrough, D.; Wachter, R. M.; Kallio, K.; Matz, M. V.; Remington, S. J. *Proc. Natl. Acad. Sci. U.S.A.* **2001**, *98*, 462.
(31) Ren, X.; Xie, D.; Zeng, J. *J. Phys. Chem. A* **2011**, *115*, 10129.
(32) Brejc, K.; Sixma, T. K.; Kitts, P. A.; Kain, S. R.; Tsien, R. Y.; Ormo, M.; Remington, S. J. *Proc. Natl. Acad. Sci. U.S.A.* **1997**, *94*, 2306.
(33) Faro, A. R.; Carpentier, P.; Jonasson, G.; Pompidor, G.; Arcizet, D.; Demachy, I.; Bourgeois, D. *J. Am. Chem. Soc.* **2011**, *133*, 16362.
(34) Roy, A.; Field, M. J.; Adam, V.; Bourgeois, D. *J. Am. Chem. Soc.* **2011**, *133*, 18586.
(35) Chattoraj, M.; King, B. A.; Bublitz, G. U.; Boxer, S. G. *Proc. Natl. Acad. Sci. U.S.A.* **1996**, *93*, 8362.
(36) Adam, V.; Lelimousin, M.; Boehme, S.; Desfonds, G.; Nienhaus, K.; Field, M. J.; Wiedenmann, J.; McSweeney, S.; Nienhaus, G. U.; Bourgeois, D. *Proc. Natl. Acad. Sci. U.S.A.* **2008**, *105*, 18343.